Stress responses and dynamic equilibrium: Key determinants of aging in the *C. elegans clk-1* mutant

Jose Carracedo-Gonzalez [1], Fausto Arellano-Carbajal [2], Etzel Garrido [3], *Roberto Alvarez-Martinez [1]

[1] Universidad Autónoma de Querétaro, Facultad de Ciencias Naturales, Laboratorio de Biología Cuantitativa y Sistemas Complejos Querétaro, Querétaro, México

[2] Universidad Autónoma de Querétaro, Facultad de Ciencias Naturales, Laboratorio de Genética Molecular y Ecología Evolutiva, Querétaro, Querétaro, México

[3] Universidad Autónoma de Querétaro, Facultad de Ciencias Naturales, Grupo de Evolución Teórica y Aplicada, Querétaro, Querétaro, México

Abstract

Systems biology is a helpful approach to study complex processes such as aging. Indeed, integrating experimental data with mathematical models and bioinformatics can help us to better understand the aging process.The long-lived mutants of *C. elegans* have generated extensive data about the molecular and cellular mechanisms involved in aging. Among these mutants, *clk-1* is a well-studied gene that encodes for a ubiquitin precursor and exhibits a pleiotropic phenotype during aging, characterized by slow rate behaviors, high levels of mitochondrial ROS, autophagy induction, and metabolic changes. However, further elucidation is required to disentangle the relationship between these molecular changes and the phenotype (lifespan extension and changes in pharyngeal pumping, swimming, and defecation). We combined experimental data and modeling tools to represent the genetic interactions with a boolean network. We then inferred the differential equations for each node –following the boolean rules– to achieve a continuous approach. The results show that *aak-2* (AMPK) is a critical gene for the long lifespan of *clk-1*, given its essential role in the induction of a stress response observed in the network attractors and the health condition and lifespan. To define the health condition of the strains (N2, *clk-1, aak-2,* and *clk-1;aak-2*), we propose a novel health index estimation based on the attrition of neuromuscular behaviors. We found that the attractor properties in the *clk-1* mutant widely depend on a cyclic regulation for the stress response. From our findings, we infer that while stress responses can increase lifespan, health primarily relies on the amount of damage.

Introduction

The nature of the aging process has captivated scientists for decades, yet its underlying mechanisms and primary drivers remain only partially understood. To elucidate these complexities, researchers have extensively employed model organisms, with the nematode *Caenorhabditis elegans* proving to be particularly useful. This worm has a mean lifespan of merely 20 days and approximately 80% of its genes have human orthologous genes (Shaye & Greenwald, 2011); *C. elegans* offers a unique window into the genetic underpinnings of aging. Particularly, mutant strains of this organism have proven invaluable for exploring the genetic modulation of lifespan. Investigations have spotlighted gene deletions that prolong life, implicating pathways such as

insulin signaling (Zhang et al., 2020), dietary restriction mechanisms (Greer & Brunet, 2009), and mitochondrial dynamics (Munkácsy & Rea, 2014). In particular, *clk-1* gene, precursor for ubiquinone synthesis, has garnered attention due to its mutation's extensive impact on both lifespan and behavioral phenotype, provoking pleiotropic effects that transcend simple metabolic adjustments (Liu et al., 2017).

Over the past quarter-century, theories attempting to elucidate the lifespan extension observed in *clk-1* mutants have ranged from the metabolic rate hypothesis (Lakowski & Hekimi, 1996) to propositions of singular regulatory processes (Durieux et al., 2011; Lapierre et al., 2013) and the more nuanced hormesis theory (Bárcena et al., 2018). Each theory contributes to our understanding yet underscores the complexity of the aging process, highlighting the need for a holistic approach to deciphering the multitude of molecular interactions and changes.

In addressing this complexity, logical modeling, mainly through constructing Boolean networks, emerges as a powerful tool. Capable of integrating diverse types of interactions, simulating system dynamics, and identifying stable states, Boolean or logical networks have been used extensively in various biological systems since their inception (Kauffman, 1969). Notable applications include replicating T cell differentiation (Mendoza, 2006), exploring mutant phenotypes in *Arabidopsis thaliana* (Espinosa-Soto et al., 2004), and evaluating pharmacological interventions (Rodríguez et al., 2012; Fumiã & Martins, 2013). This modeling approach holds particular promise for unraveling the *clk-1* mutant paradox, where reduced ubiquinone levels and resultant ROS accumulation paradoxically extend lifespan, suggesting a complex interplay of molecular interactions awaiting integration into a comprehensive model.

A unique advantage of logical modeling is its ability to simulate perturbations, mirroring mutant conditions such as the *clk-1;aak-2* double mutant, which reverses the lifespan extension of *clk-1*. This mutation, affecting the AMPK kinase alpha subunit, modifies behaviors like the pharyngeal pumping rate, offering insights into the subtle relationship between genetic mutations, lifespan, and healthspan (Curtis et al., 2006). While lifespan extension in mutants is noteworthy, alterations in behavior highlight the relevance of healthspan — the period of life spent in good health — which remains challenging to quantify due to its subjective nature and the difficulty in pinpointing the transition to functional decline (Tissenbaum, 2012; Kaeberlein, 2018).

Here, we adopt a systems biology approach to dissect the phenotypic outcomes of single-gene mutations in *clk-1* and the *clk-1;aak-2* double mutant through logical modeling. By analyzing discrete and continuous system dynamics to identify attractors and correlating these with measured behaviors such as pharyngeal pumping, swimming, and defecation, we aim to establish a comprehensive health condition profile for these strains. We proposed a novel health index estimation based on the overall decline in behaviors over nine days; we seek to elucidate the intricate relationship between single-gene mutations, lifespan, health condition, and the underlying molecular interactions that regulate these phenomena.

This study aimed to comprehend the aging process by constructing a discrete boolean network based on an extensive literature review from the last three decades. The steady states of this network were analyzed through a discrete and continuous approach using evidence about the expression levels to validate the model. They set the molecular landscape for the lifespan and health

condition phenotypes. This study employed a quantitative approach to unveil the relationship between the model and the *in vivo* data, illuminating the role of stress response in the aging process and the dynamic nature of this process.

Nuevo párrafo que combina los dos

Here, we adopt a systems biology approach to dissect the phenotypic outcomes of single-gene mutations in *clk-1* and the *clk-1*;*aak-2* double mutant through logical modeling. By analyzing discrete and continuous system dynamics to identify attractors and correlating these with measured behaviors such as pharyngeal pumping, swimming, and defecation, we aim to establish a comprehensive health condition profile for these strains. We proposed a novel health index estimation based on the overall decline in behaviors over nine days; we seek to elucidate the intricate relationship between single-gene mutations, lifespan, health condition, and the underlying molecular interactions that regulate these phenomena. This study aimed to comprehend the aging process by constructing a discrete Boolean network based on an extensive literature review from the last three decades. The steady states of this network were analyzed through a discrete and continuous approach using evidence about the expression levels to validate the model. They set the molecular landscape for the lifespan and health condition phenotypes. This study employed a quantitative approach to unveil the relationship between the model and the in vivo data, illuminating the role of stress response in the aging process and the dynamic nature of this process.

Materials and Methods

Construction and Analysis of the *clk-1* Regulatory Network Model

We have built a comprehensive model for the *clk-1* regulatory network. To achieve this, we thoroughly researched the existing literature to gather all documented interactions relevant to *clk-1*. Our goal was to include a complete set of interactions to ensure that the model accurately reflects the current understanding of this organism model. The outcome of this effort is inferring a regulatory network, a structured representation that encapsulates the relationships of molecular interactions within the *clk-1* network.

In this regulatory graph, each node symbolizes a distinct molecular component, such as genes, proteins, or small molecules, integral to the *clk-1* network. The edges that connect these nodes denote the regulatory influence — positive or negative — one component exerts on another. These relationships are not arbitrary; they are grounded in logical rules derived from empirical observations and theoretical underpinnings, allowing for predicting node activity levels based on the interplay of regulatory signals.

We utilized the Cytoscape software (Institute for Systems Biology, 2019, Version 3.9.1) to visualize the biological network depicted in the graph. Through Cytoscape, we represented the *clk-1* regulatory graph in a user-friendly format, facilitating a simplified exploration of its structure and dynamics. Furthermore, we enhanced the precision and predictive capability of the model using the R-package BoolNet (Müssel et al., 2010). This package was the computational framework for

simulating the *clk-1* network and identifying its stable states. These are crucial in representing network configurations that may endure over time, potentially correlating with specific phenotypes.

Additionally, we utilized the R-package BoolNetPerturb (Martinez-Sanchez & Arias Del Angel, 2022) to simulate the effects of various perturbations on the *clk-1* network, gaining valuable insights into its resilience and adaptability. Furthermore, the DeSolve R package (Soetaert et al., 2010) allowed us to delve into the network's continuous dynamic behaviors, leading to a more comprehensive understanding of its temporal dynamics under different conditions.

C. elegans strains and culture

Nematodes were cultured in standard conditions on Nematode Growth Medium (NGM) plates and fed with the *Escherichia coli* strain OP50 at 20°C temperature (Brenner, 1974). In these experiments, the wild-type strain used was Bristol N2. Mutant strains included *aak-2(ok524)* and *clk-1(qm30)*. The strains were provided by the CGC, which is funded by NIH Office of Research Infrastructure Programs (P40 OD010440). To create a double mutant, *aak-2(ok524)* males were crossed with *clk-1(qm30)* hermaphrodites. F2 progeny were then separated on individual plates to identify the double mutants using the polymerase chain reaction (PCR) technique. To identify the *aak-2* mutation, the following primer sequences were utilized: forward TTCCTGGCAACACCATAAGC and reverse CTCCAGAAAGTCTGGAGTTG. On the other hand, to detect the *clk-1* mutation, the primer sequences used were forward TGTCGGTTCAGCACTTCTAG and reverse AGTATTGTCCGTGTCAGGAC. This method allowed for precise identification and analysis of the desired genetic configurations, contributing significantly to our knowledge of nematode genetics.

Measurement of Neuromuscular Behaviors

Our study assessed neuromuscular behaviors using the methodologies outlined by Hart (2006), focusing on a trio of specific behaviors: pharyngeal pumping, swimming, and defecation. These behaviors were selected as indicators of neuromuscular activity and coordination, offering insights into the nematodes' physiological health and functional status under investigation.

The experimental protocol commenced with nematodes that had reached one day of adulthood. A cohort of 20 worms was selected to ensure age and developmental stage uniformity. This selection criterion was crucial for minimizing variability in neuromuscular function that might arise from differences in maturation. The behaviors of these worms were then systematically observed and recorded over nine days, with assessments conducted at 48-hour intervals. This longitudinal approach allowed us to capture possible changes in neuromuscular activity over time, providing a comprehensive overview of each behavior.

We measured pharyngeal pumping and swimming behaviors, involving three independent replicates for each worm at every observation point. Pharyngeal pumping, a critical indicator of feeding behavior and metabolic activity, was quantified by counting the number of contractions within a predefined time frame (30 seconds). Swimming behavior, reflecting motor coordination and muscle function, was evaluated based on the worms' mobility and the fluidity of their movements in an aquatic environment. During each observation session, the defecation behavior of each worm was measured with a single replication. We recorded defecation cycles, characterized by

periodic expulsion events, to gain insight into the regulation of the gastrointestinal and neuromuscular systems.

Survival analysis

Our survival analysis protocol was designed following the procedures delineated by Park et al. (2017) to ensure the reliability and reproducibility of our results. This approach allowed for the precise monitoring of nematode longevity under controlled conditions. The experimental setup began with selecting nematodes at the L4 larval stage, an easily identifiable stage in their development. These selected individuals were then carefully transferred onto fresh Nematode Growth Medium (NGM) plates. This transfer was performed to standardize the starting conditions for each nematode, thereby reducing variability in survival outcomes that might arise from differences in environmental factors or developmental stages at the onset of the assay.

Twenty-four hours post-transfer, marking the transition of the nematodes to one-day adults, the survival assays officially commenced, with this time point designated as $t = 1$. This initiation at the adult stage ensured that the survival data captured pertained exclusively to the adult phase of the nematode life cycle, facilitating focused analysis on adult longevity.

We monitored the schedule during the survival assays, with assessments conducted every 24 hours. Nematodes that deviated from the experimental parameters, such as those that crawled off the plate, exhibited bagging (a condition where eggs hatch inside the mother, leading to her death), or exploded, were censored at the time these events were observed. The censoring of these individuals was critical for the integrity of the survival analysis, as it accounted for non-standard mortality causes that do not directly relate to the natural lifespan of the organism. The nematodes were transferred to new NGM plates every 48 hours to maintain optimal conditions and minimize confounding factors such as overcrowding or depletion of food resources. This bi-daily transfer protocol was pivotal in ensuring that environmental degradation did not influence the observed survival outcomes over time. Additionally, this strategy prevented the inadvertent inclusion of new adults from potential reproduction, thus maintaining the purity of the adult cohort under study.

Health index estimation

In our study, we developed a nuanced approach to estimate the health index of nematodes, leveraging the dataset derived from our behavioral analyses. This estimation process was designed to encompass individual and aggregated behavioral metrics, providing a holistic view of the nematodes' physiological state over time.

Aggregation of Behavioral Data into a Health Index

We first standardized the behavioral data to construct the health index by converting it to a relative scale. This standardization facilitated the comparison and aggregation of diverse behaviors on a standard metric, enhancing the interpretability of our analysis. Data from different behaviors were cumulatively added for the aggregation process to form a composite score. Notably, in the case of defecation—a behavior that increases its length over time—its relative metric was subtracted from the composite of the other behaviors. This adjustment was crucial for accurately reflecting the contribution of each behavior to the overall health index, acknowledging that not all behaviors equally signify healthiness.

Symbolic Regression for Health Index Estimation

The initial method employed for estimating the health index was symbolic regression, executed through the software Eureqa (version 1.24.0, 2015). Symbolic regression diverges from traditional regression by searching for the mathematical expression that best fits the relationship within the data rather than fitting the data to a predefined model. Through this process, we identified the optimal function that exhibited the highest fidelity to the behavioral data patterns. Following identifying this function, we calculated its definite integral over the observed period. This integral, representing the area under the curve generated by the function, served as a quantitative measure of the cumulative health index across the lifespan of the nematodes.

Direct Area Calculation from Behavioral Data

Additionally to the symbolic regression approach, we employed a direct method to estimate the health index by calculating the area under the data curve. This method drew lines through the behavioral data's first, second, or third quartiles for each measurement day. By connecting these points across the observation period, we delineated polygons whose boundaries were defined by the quartile lines and the temporal axis representing the consecutive days. The area enclosed by these polygons was then computed, offering an alternative measure of the health index that is directly derived from the raw behavioral data.

Statistical analysis

In our study, the statistical analysis assessed the effects of genetic variation and temporal dynamics on neuromuscular behaviors and evaluated survival patterns across different nematode strains. We employed a two-fold statistical approach, incorporating a two-way mixed Analysis of Variance (ANOVA) and Cox proportional hazards regression analysis, to dissect the nature of these effects.

Two-Way Mixed ANOVA for Neuromuscular Behavior Analysis

The two-way mixed ANOVA was specifically chosen for its capability to simultaneously evaluate the influence of two independent variables—namely, nematode strain (a between-subjects factor) and time (a within-subjects factor)—on the measured neuromuscular behaviors. This analysis facilitated the discernment of strain-specific behavioral profiles and their progression over time, allowing us to pinpoint any significant deviations attributable to genetic differences or temporal changes.

The implementation of the two-way mixed ANOVA was conducted to evaluate the interaction effect between strain and time, providing insights into whether the impact of genetic variation on neuromuscular behavior changes over the lifespan of the nematodes.

Cox Proportional Hazards Regression for Survival Analysis

The Cox proportional hazards regression model was employed to analyze survival data. This statistical technique was selected for its capacity to compare survival curves across different strains of nematodes while accounting for potential confounders. Using the Cox model, we could estimate the hazard ratios, offering a quantifiable measure of the risk of mortality associated with each strain relative to the wild-type under the assumption of proportional hazards over time.

The Cox regression analysis was performed to verify the proportionality of the hazard assumption, employing both graphical diagnostics and statistical tests. This step ensured the validity of the model's findings. The survival curves generated from this model were then statistically

compared, with the resulting p-values providing a basis for assessing the significance of differences observed between strains.

Results

The boolean network integrates all the known interactions for the *clk-1* mutant

To construct a model of the regulatory network in *Caenorhabditis elegans*, we conducted an extensive review of the literature, focusing on publications related to *clk-1* and similar mitochondrial mutants. This thorough survey was crucial for gathering a dataset encompassing all the molecular interactions associated with the *clk-1* phenotype. The resulting model, depicted in Figure 1, incorporates 29 distinct molecular components and 46 specific interactions. These components span a variety of biological entities, including individual proteins and entire metabolic pathways, illustrating the diverse nature of the *clk-1* regulatory network (as detailed in Table 1). The model depicts key processes such as mitochondrial unfolded protein response (UPRmt), autophagy, mitochondrial fusion, and lipid metabolism, emphasizing the wide range of cellular mechanisms influenced by *clk-1* mutations.

Based on empirical evidence, each interaction was encoded using logical rules to translate the *clk-1* interactions into a functional model (referenced in Table 1). This approach enabled the computational simulation of the network's behavior, providing insights into the dynamic interplay among the components. A particularly complex aspect of the model is the feedback loop involving AMP-activated protein kinase (AMPK), reactive oxygen species (ROS), and hypoxia-inducible factor 1 (HIF-1). The density of interactions within this loop presents significant challenges for simulating the network's dynamics, necessitating the adoption of a discrete synchronous update model to manage the computational complexity.

Figure 1

Given the complexity observed in the feedback loop among AMPK, ROS, and HIF-1, we opted to implement two distinct configurations to accurately model the interactions between these critical elements. The first configuration adopts a simplified approach, focusing on the minimal interactions required to activate or inhibit the elements. This configuration was designed to reduce the model's complexity, enabling a clearer understanding of the fundamental mechanisms (Figure 2 A and C). The other configuration contemplates the whole interactions as described by the literature; this is

biologically more accurate, but it is not feasible for the discrete model, due to the constant positive and negative interactions among these elements (Figure 2 B and C).

Figure 2

This dual-configuration strategy underscores our commitment to accurately capturing the nuances of the *clk-1* regulatory network, acknowledging the need for flexibility in modeling approaches to accommodate the inherent complexity of biological systems. Through this detailed examination of the *clk-1* interactions and the strategic implementation of modeling techniques, we aim to shed light on the underlying regulatory mechanisms contributing to the *clk-1* mutant's unique phenotype, offering valuable insights into the broader context of mitochondrial function and its implications for cellular aging.

Table 1

The long lived mutant attractors show upregulation in all processes

The steady states of the model are called attractors and, in a discrete approach, these attractors are the states, or combinations of states, where all the other possible states are led. For configuration 1, in the wild type (N2 strain) conditions, the value of *clk-1* is always 1 (active) and 100% of the states drive to a single state attractor where all the main processes are inhibited (Figure 3A), but in mutant conditions when the *clk-1* value is always 0 (inactive) the main attractor is composed of 16 states where all the processes are oscillating between active and inactive (Figure 3B), also a 78% of all possible states led to this attractor. Besides this result, two more cyclic attractors of 11 and 10 states exist in the *clk-1* mutant conditions (Figure S1). These attractors show the same result as the 16-state attractor, where all the processes oscillate.

The other condition tested is the *clk-1;aak-2* double mutant, where the *clk-1* and AMPK value is always 0; the two resulting attractors show a static condition similar to the wild type attractor, unlike this condition, the elements associated with the UPRmt are oscillating. Also, the elements *pink-1* and *skn-1* are activated (Figure 3C), and both attractors have a basin of attraction close to 50%. These results so far were obtained for configuration 1 in a discrete approach, the major difference within the first and second configuration pivot on the *clk-1* mutant conditions. While configuration 1 throws feasible attractors, configuration 2 throws a set of 10 cyclic attractors, and none of those cyclic attractors contemplates the electric transport chain compensation (Figure S2). In addition to this condition, both configurations' attractors for the double mutant and the wild-type conditions are the same.

The discrete attractors for configuration 1 show a better simulation of the *clk-1* mutant conditions. We found that the inductor of UPRmt, the *atfs-1* transcription factor, increases its expression in this mutant (Wu et al., 2018); for the autophagy process, the *hlh-30* transcription factor increases its expression (Lapierre et al., 2013), in the case of mitochondrial fusion there is an increase in the number of elongated mitochondria as well as an expression increase of the mitofusins *eat-3* and *fzo-1* (Chaudhari & Kipreos, 2017), finally a microarray analysis revealed that the genes involved in fatty acid oxidation increase their expression (Long & Kim, 2021).

Figure 3

The continuous approach might shows a better representation of the system

In the continuous approach, the logical rules are fitted into ordinary differential equations with sigmoidal functions; each element can constantly change its activation state according to the combination of positive and negative interactions. For configuration 1, the continuous attractor shows a constant oscillation for each element (except for the static elements in the discrete approach) (Figure 4A); some groups of elements in this configuration show an oscillation pattern where these groups are activated and inhibited at the same time (Figure S3). On the other hand, configuration 2 shows a more feasible result than the discrete approach, in this configuration, the elements reach a steady state on a static value between 0 and 1, but in most of the cases is not 0 or 1 (Figure 4B and S2B). This result could be an artifact of the model; to prove this, further research is required. While configuration 2 might reflect the general expression level, configuration 1 may reflect the expression dynamics at a single cell level. These stable states are particularly interesting as they represent the network configurations that can persist over time, potentially correlating with specific phenotypes.

Figure 4

The healthspan is unrelated to lifespan

The lifespan was measured through a survival assay, we found that N2, *aak-2* and *clk-1;aak-2* have a shorter lifespan than *clk-1* worms (Figure 5), a Cox regression analysis revealed that there is a significative difference between N2 and the strains *aak-2(ok524)* and *clk-1(qm30),* but not with the strain *clk-1(qm30);aak-2(ok524),* also there is a 71.5% less risk of death for the *clk-1* concerning the strain N2.

Figure 5

We proposed a novel estimation of a health index based on the general muscular attrition in *C. elegans* to measure its health condition. This variable is measured in 1-day adult worms until they reach the 9-day age and is through the behaviors of pharyngeal pumping, swimming, and defecation. We found significant differences between strains and measurement times for individual and aggregated behaviors (Figure S4).

We implemented two methods to estimate the health index. The first one is based on symbolic regression estimation. This method uses a genetic algorithm to calculate the best function that fits the data, and then we took the definite integral of this function to measure the area under the curve. Below is shown an example of this kind of calculation using for the N2 data estimated function.

$$\int_{1}^{9} (1.72 - 0.08X - 0.06\cos(4.95 - X))\, dx = 10.38$$

The second method is a direct measurement from the data; we defined a line through the points established by the quartiles of each day's measurement, and then we calculated the area of the polygons defined by this line and the distance between measurements, as shown in Figure S5. The area under the function, or the quartiles, reflects the general attrition. If the behavior keeps high and healthy longer, the area (index) will be bigger, but if the behavior is slow and decays quickly, the index will be smaller.

The results show that strain N2 has a higher health index (therefore the best health condition), and strain *aak-2(ok524)* is close to this value. On the other hand, the long-lived strain *clk-1 (qm30)* has almost half of this value, and the double mutant *clk-1(qm30);aak-2(ok524)* is closer to a quarter of the N2 value (Table 2). The general result is replicated in any aggregate of behaviors as well as in individual behaviors (Table S1), despite this information, the more behaviors measured are aggregated to the health index, the bigger the impact shown on ill strains, and the health condition of the strains is not as positive as their lifespan. We also checked which strains had the greatest deterioration according to their initial conditions; the result between strains was the same, but there were slight differences (Table S2). Regarding the two methods used, the quartile 2 calculated area fits the symbolic regression estimated area (Tables 2, S1, and S2), this makes the area calculation method more accurate than the symbolic regression method but makes the regression method more useful for longitudinal studies where the data is a cloud of points.

Discussion

Until now, most wet lab studies about the aging process have focused on single gene interactions, ignoring the underlying molecular network or the health condition and lifespan status, in the case of computational modeling. This work aims to address these limitations by first inferring the molecular network involved in the *clk-1* aging phenotype and then testing the boolean model to identify the steady state conditions for relevant genes in this mutant. Subsequently, using bioassays and a novel health index estimation, we established the lifespan and health condition for the relevant mutants tested in the boolean model. This comprehensive approach enabled us to elucidate some of the regulatory dynamics involved in the aging process.

The study suggests that under certain conditions, such as those involving the mitochondrial mutant *clk-1,* various processes are triggered that indicate a stress response. This stress response was partially or completely inhibited in the wild-type and double mutant of *clk-1* and *aak-2* strains, respectively (Figures 3A and 3C). In these conditions, both strains had similar lifespans (Figure 5), implying that the stress response is involved in the *clk-1* mutant lifespan extension (Figures 3B and 5). .On the other hand, health index results showed a decreased health condition for the *clk-1* mutant (Table 2), contradicting the hormesis theory (Bárcena et al., 2018). However, the adverse condition still had a beneficial effect in lifespan.

In contrast, the double mutant *clk-1;aak-2* did not have a long lifespan or good healthspan (Figure 5 and Table 2), which can be attributed to the absence of cell repair and the increased levels of reactive oxygen species. These findings indicate that the lifespan of *C. elegans* is dependent on its stress response and the subsequent metabolic, epigenetic, and cellular changes that occur. However, healthspan is only affected by the amount of cellular stress and how well it is managed.

Estimating a health index is useful for measuring the health condition in this study. It does not assume a specific shift from healthy to ill, providing a more comprehensive view of health. This

index reflects the development of sarcopenia, influenced by muscular attrition and behavior. It can occur in the *clk-1* mutant strain despite its initial slow rate of behavior, which does not slow down metabolism and increases lifespan (Bansal et al., 2015), therefore, slow behavior is linked to the development of sarcopenia in these strains. Regarding the model, one noteworthy aspect of the attractors obtained is their cyclic properties, which may be an approximation of the theory of homeodynamics (Yates, 1994). This suggests that biological systems are not static and should be studied as complex processes with emergent properties. Aging is a complex process due to its hierarchical structure and how the healthy or frail condition emerges as an emergent property of molecular and cellular dynamic interactions (Cohen et al., 2022). Under this assumption, cyclic attractors can be interpreted as a form of dynamic equilibrium from which lifespan and health condition phenotypes emerge. For this model, defining the dynamic balance that regulates the conditions of *clk-1*, including all metabolic, epigenetic, and proteostatic factors, and determining whether the N2 attractor remains static with the appropriate information and how a cyclic attractor changes over time would be necessary.

Analyzing the aging process as an emergent property of homeodynamics might bring us closer to defining an aging paradigm, as the hallmarks of aging have been identified thus far (López-Otín et al., 2013). Understanding the role of each molecular factor and its contribution at the primary or secondary level is essential for defining a paradigm of aging (Gems & De Magalhães, 2021), and logical modeling provides an excellent tool for integrating and analyzing these factors as a dynamic complex process. Nonetheless, it is crucial to demonstrate that gene expression correlates with cyclic attractors and follows a homeodynamic pattern. To achieve this, it would be necessary to measure genetic expression at the cellular level.

Conclusionsº

In our research, we have employed logical modeling and quantitative methods to investigate the intricate relationship between the processes associated with the *clk-1* mutant and its aging phenotypes. This comprehensive approach has enabled us to elucidate the potential homeostatic properties of the aging process, highlighting the critical role of stress responses and dynamic equilibrium as key regulators of lifespan. Our findings indicate promising directions for future exploration in this domain.

Estimating the health condition using a health index provided a comprehensive view, reflecting sarcopenia development influenced by muscular attrition and behavior. The cyclic properties of the attractors in the model suggest a homeodynamic theory, which posits that homeostasis is not a static process as the name suggests, but a dynamic system where all the metabolites are constantly changing in concentrations and interactions , how these changes evolve along time may explain the aging process

Analyzing aging as an emergent property of homeodynamics may help define an aging paradigm, as identifying primary and secondary aging causes remains challenging due to the scale of the

dynamics aforementioned, and the complex system properties of this process. Logical modeling is valuable for integrating and analyzing molecular factors as a dynamic process. However, demonstrating gene expression correlation with cyclic attractors and homeodynamic patterns requires precise cellular-level measurements using advanced technologies .

Acknowledgments

We thank FONDEC-UAQ 2022 (20205007011001) for their financial support. Additionally, we acknowledge CONAHCyT for providing a Master's degree stipend.

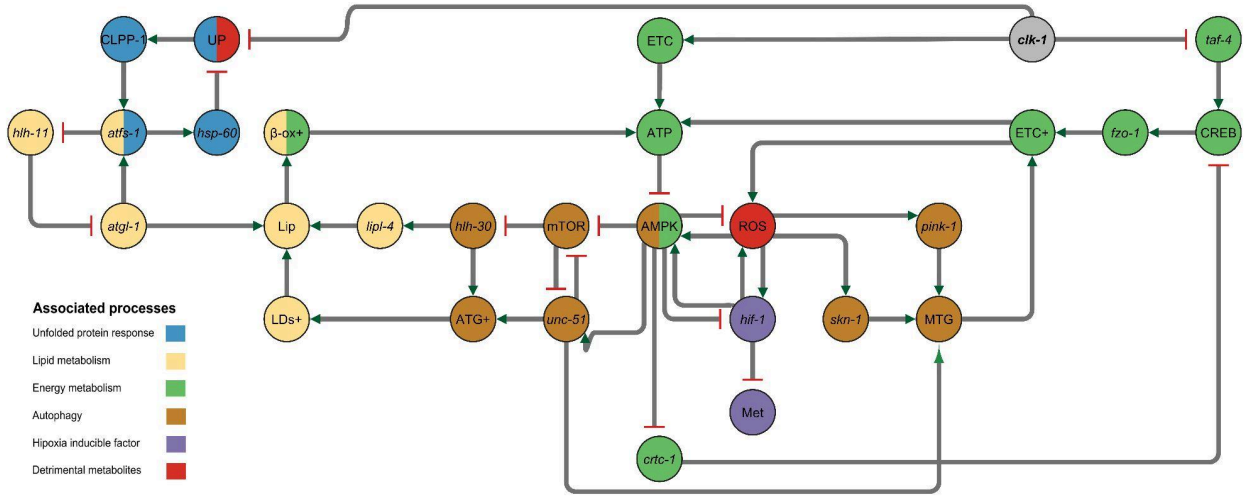

Figure 1. Logical regulatory network of *clk-1* mutant molecular interactions. The model was designed to study the regulatory landscape in the *C. elegans clk-1* mutant. The nodes are divided into six categories: UPRmt nodes, lipid metabolism nodes, energy metabolism nodes, autophagy nodes, hypoxia response nodes, and detrimental metabolites nodes. A color code denotes these categories. The arcs connecting the nodes represent positive (green arrow) or negative (red line) regulatory interactions.

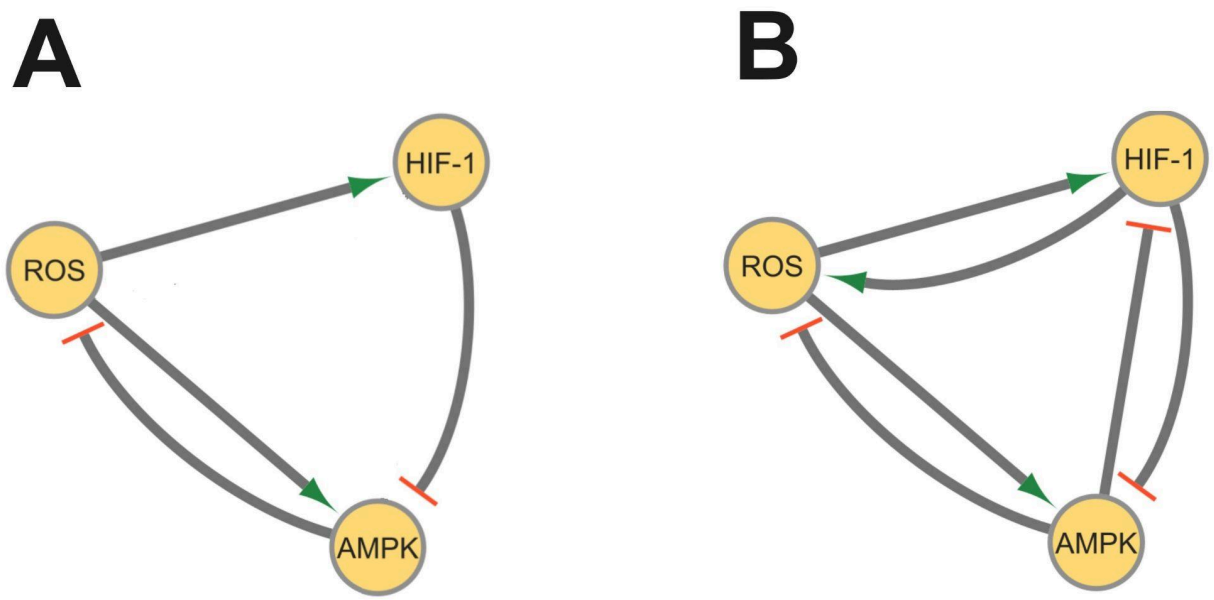

C

Element	Boolean rules	
	Configuration 1	Configuration 2
ROS	**ETC2** or (not **AMPK** and not **CLK-1**)	not **ETC** and (not **AMPK** or **HIF-1**)
HIF-1	**ROS**	**ROS** and not **AMPK**
AMPK	not **ATP** or (**ROS** and not **HIF-1**)	**ROS** and not **HIF-1**

Figure 2. The dual-configuration for the ROS, HIF-1 and AMPK loop. For a better depiction of the system in a discrete model it was necessary to establish a new and simpler configuration (A). Graph of the configuration 1 (the simpler configuration) for the *clk-1* network (B). Graph of the configuration 2 (the accurate configuration) for the *clk-1* network (C). Boolean rules for both configurations.

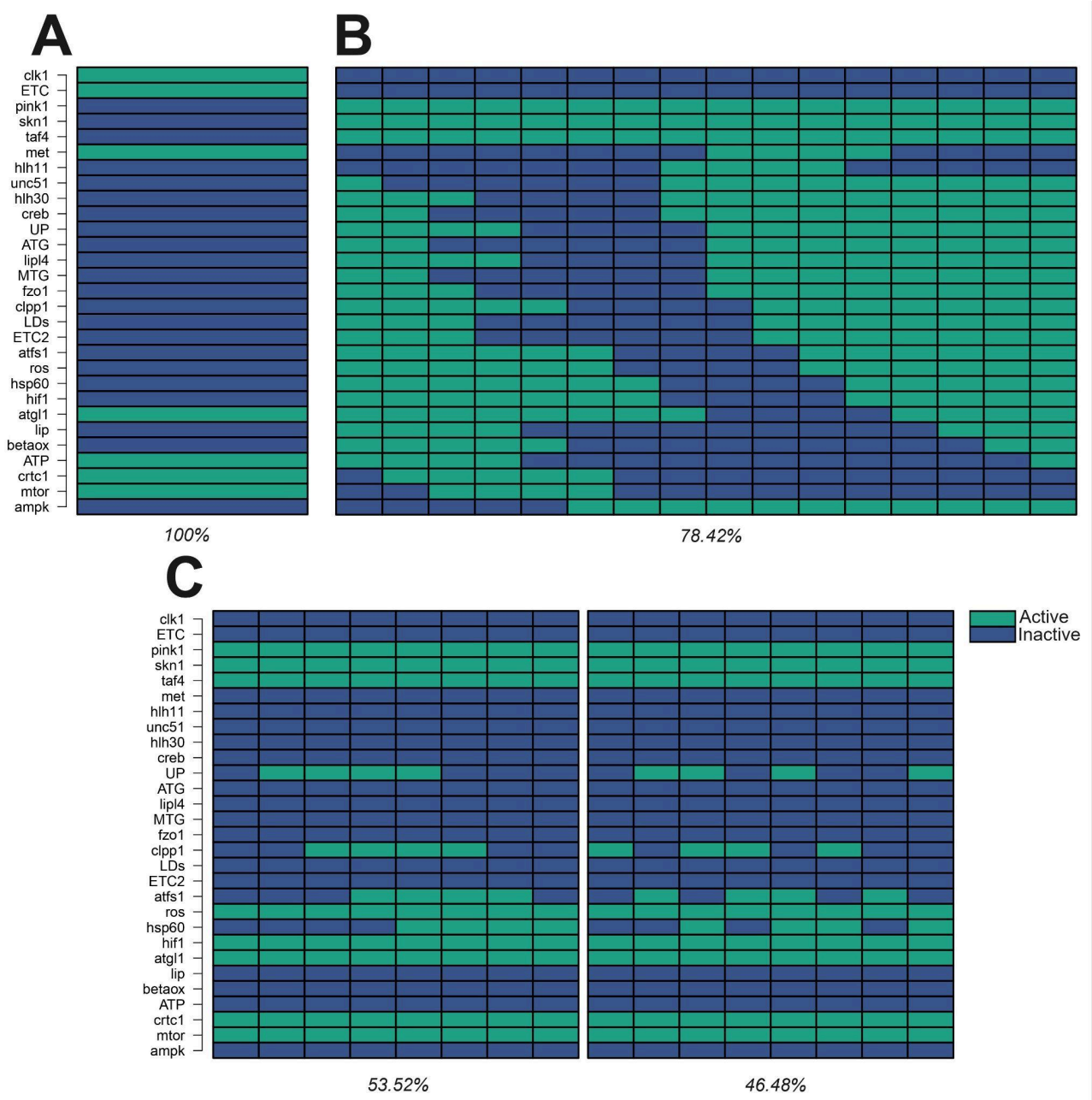

Figure 3. The logical modeling analysis reflects the impact of molecular interactions on mutant strains. Computation of the attractors for all nodes of the model in three different conditions: columns are the states and lines the nodes, A color code denotes each node state, active (green) or inactive (blue) at the bottom of each attractor is shown its basin of attraction (A). Static attractor for the wild type N2 condition (B). Main cyclic attractor for the *clk-1* mutant condition (C). The two cyclic attractors for the double mutant *clk-1;aak-2* condition.

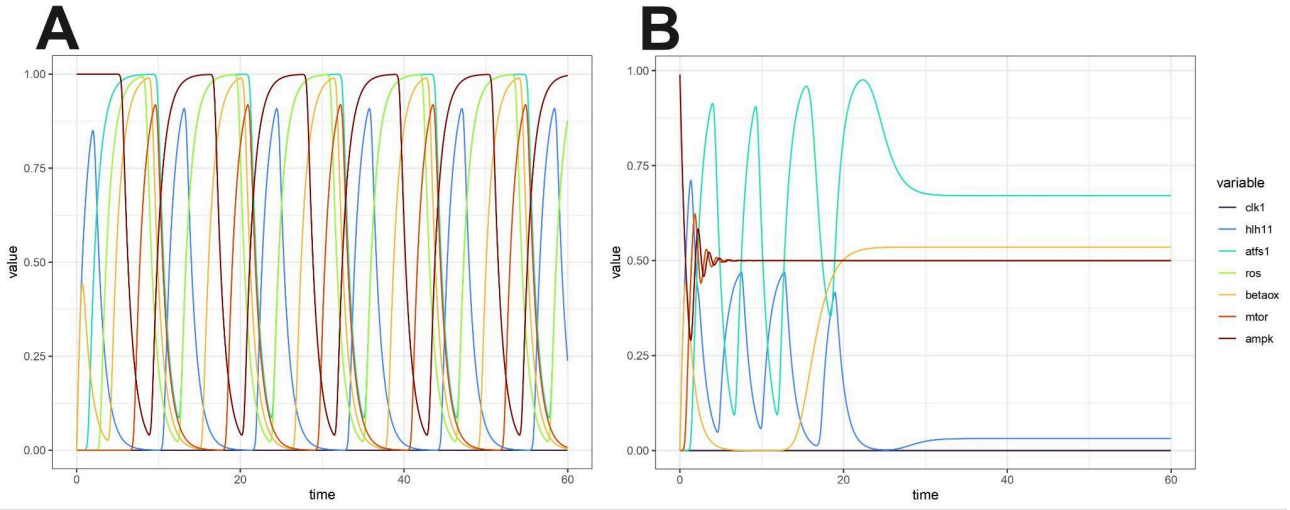

Figure 4. Configuration 2 has a static attractor for the *clk-1* mutant condition in the continuous approach. Computation of the stable states on selected nodes of the model in the *clk-1* mutant condition, each line depicts a node. The Y axis shows the activation level between 0 (inactive), and 1 (active) and the X axis shows the time. (A) The continuous simulation for the configuration 1 cyclic attractor (B) The continuous simulation for the configuration 2 static attractor.

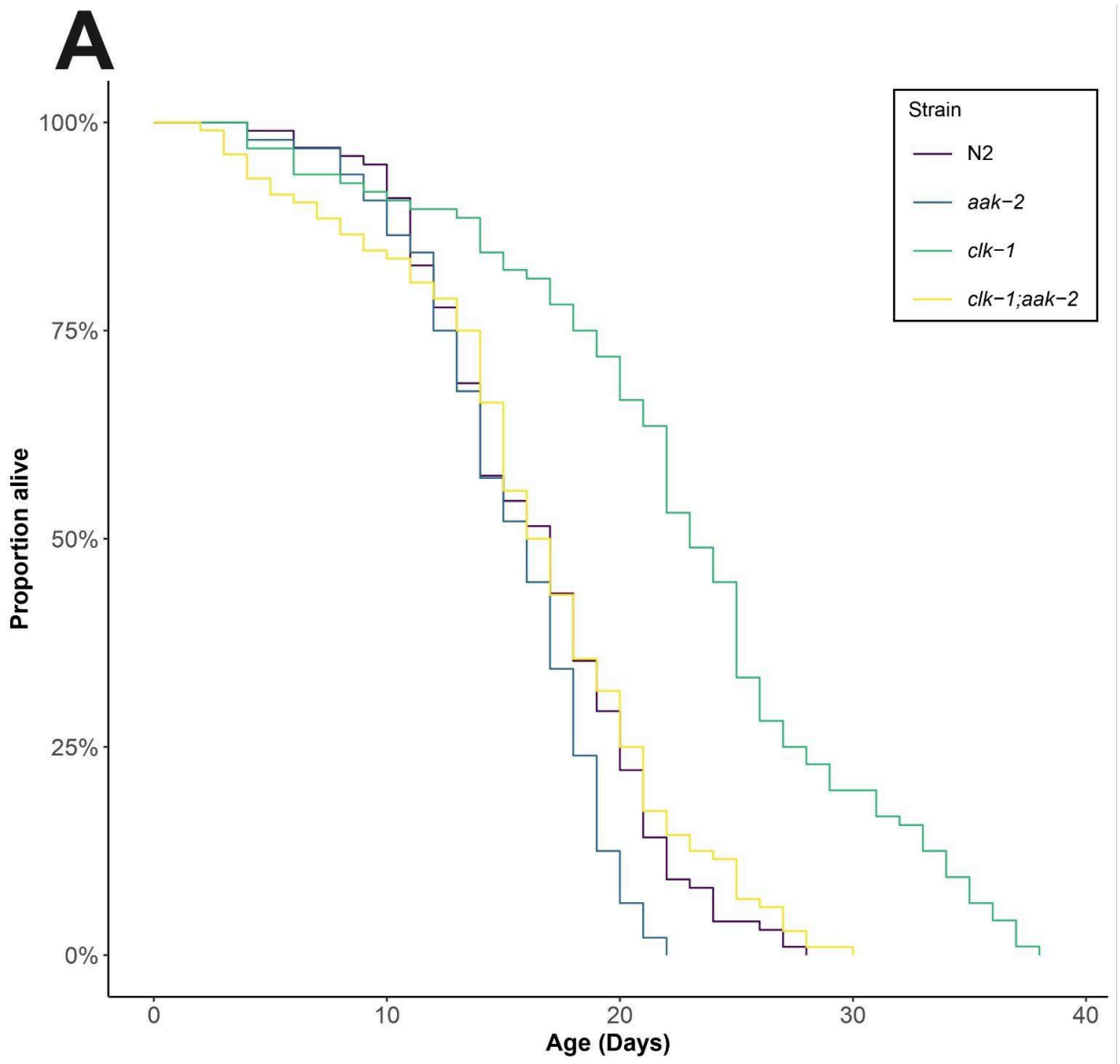

B

Strain	Regression coefficient	Risk ratio	Coefficient standard error	*Z* value	*P* value
aak-2	0.3890	1.4755 (-47.5%)	0.1462	2.661	0.007**
clk-1	-1.2552	0.2850 (71.5%)	0.1613	-7.78	7.24e-15***
clk-1;aak-2	-0.1377	0.8714 (12.8%)	0.1411	-0.976	0.329

Figure 5. Only the *clk-1* strain has a positive effect on lifespan. (A) Survival curve of all strains used in this study: wild type (N2) (purple), *aak-2(ok524)* (blue), *clk-1(qm30)* (green), and *clk-1(qm30);aak-2(ok524)* (yellow). (B) Cox regression analysis based on the hazard ratio of the mutant strains compared with the wild type. The significance codes are the following: P = 0, '***'; P < 0.001, '**'; P < 0.01, '*' and, " ", non-significant.

Table 1: Network components and their interactions. Logical rules are defined in boolnet nomenclature.

Element	Element description	Logical rule	References of interactions
clk-1	Ubiquinone precursor	0	(Liu et al., 2017)
ETC	Electric transport chain	ETC, clk1	(Munkácsy & Rea, 2014)
pink-1	Kinase	pink1, !ETC	(Palikaras et al., 2015) (Palikaras et al., 2015)
skn-1	Transcription factor	skn1, ros | !ETC	(Palikaras et al., 2015) (Palikaras et al., 2015)
taf-4	Transcription factor	taf4, !clk1	(Khan et al., 2013)
Met	Methionine	met, !hif1	(Choi et al., 2021)
hlh-11	Transcription factor	hlh11, !atfs1 & !mtor	(Li et al., 2020) (Littlejohn et al., 2020)
unc-51	Kinase	unc51, ampk & !mtor	(Corona Velazquez & Jackson, 2018) (Alers et al., 2012)
hlh-30	Transcription factor	hlh30, !mtor	(Antikainen et al., 2017)
CREB	Transcription factor	creb, taf4 & !crtc1	(Khan et al., 2013)
UP	Unfolded proteins	pmp, !clk1 & (ETC2 | !hsp60)	(Van Raamsdonk et al., 2010) (Wiedemann & Pfanner, 2017) (Barcelos & Haas, 2019)
ATG	Autophagy	ATG, unc51 & hlh30	(Lapierre et al., 2013) (Nakamura & Yoshimori, 2018)
lipl-4	Lapase	lipl4, hlh30	(Antikainen et al., 2017)
MTG	Mitophagy	MTG, pink1 & skn1 & unc51	(Palikaras et al., 2015) (Nakamura & Yoshimori, 2018)
fzo-1	Mitochondrial fusion protein	fzo1, creb	(Mayr & Montminy, 2001)
clpp-1	protease	clpp1, pmp	(Haynes et al., 2007)
LDs	Lipid droplets	LDs, ATG	(Nguyen et al., 2017) (Mailler et al., 2021)
ETC+	Compensatory electric transport chain	ETC2, fzo1 & MTG	(Youle & van der Bliek, 2012) (Hernando-Rodríguez & Artal-Sanz, 2018)
atfs-1	Transcription factor	atfs1, clpp1	(Wu et al., 2018)

ROS	Reactive oxygen species	ros, !ETC & (!ampk | hif1)	(Bentinger et al., 2007) (Hwang et al., 2014) (Wang & Hekimi, 2019)
hsp-60	Heat shock protein	hsp60, atfs1	(Wiedemann & Pfanner, 2017) (Wu et al., 2018)
hif-1	Hipoxia inducible factor	hif1, ros & !ampk	(Khan et al., 2013) (Hwang et al., 2014)
atgl-1	Lipase	atgl1, !hlh11	(Littlejohn et al., 2020)
lip	Lipids	lip, lipl4 & LDs & atgl1	(Zaarur et al., 2019) (Littlejohn et al., 2020) (Mailler et al., 2021)
β oxidation	Beta oxidation	betaox, lip	(Zaarur et al., 2019)
ATP	Adenosine triphosphate	ATP, (ETC2 & betaox) | ETC	(Van Raamsdonk et al., 2010)
crtc-1	transcription coactivator	crtc1, !ampk	(Khan et al., 2013)
mTOR	Kinase	mtor, !ampk & !unc51	(Corona Velazquez & Jackson, 2018) (Alers et al., 2012)
AMPK	Kinase	ampk, (ros & !hif1)	(Hwang et al., 2014)

Table 2. Health index estimation. The area from the symbolic regression method was calculated through the definite integral of each estimated function, and the area from the quartiles was calculated from the polygons drawn by the data quartiles of each day.

Strain	Symbolic regression estimation			Area under the quartiles		
	Regression function	**Area**	**%**	**Q1**	**Q2**	**Q3**
Pharyngeal pumping and swimming index						
N2	$Y = 1.65 + 0.05\sin(6.03 + X) - 0.06X$	10.91	100%	10.028	10.896	11.639
aak-2	$Y = 1.73 + 0.01/\sin(X) - 0.08X$	10.55	96.7%	10.12	10.699	11.469
clk-1	$Y = 1.28 + 4.62e^{-11}X(X^X) - 0.11X$	5.84	53.52%	5.139	5.966	6.95
clk-1;aak-2	$Y = 97.2/(33.57 + X) - 2.12$	3.25	29.78%	2.44	3.263	3.971
Pharyngeal pumping, swimming and defecation index						
N2	$Y = 1.72 - 0.08X - 0.06\cos(4.95 - X)$	10.38	100%	9.299	10.279	10.896
aak-2	$Y = 1.83 + 0.06\cos(1.8X) - 0.11X$	9.94	95.76%	9.416	10.03	10.662
clk-1	$Y = 0.57 + 0.63\sin(X^2)$	4.8	46.24%	2.018	3.105	4.179
clk-1;aak-2	$Y = 0.71 - 0.1X - 6.32e\text{-}6X^5$	1.06	10.21%	1.214	1.738	2.249

References

Alers, S., Löffler, A. S., Wesselborg, S., & Stork, B. (2012). Role of AMPK-mTOR-Ulk1/2 in the Regulation of Autophagy: Cross Talk, Shortcuts, and Feedbacks. Molecular and Cellular Biology, 32(1), 2–11. https://doi.org/10.1128/MCB.06159-11

Antikainen, H., Driscoll, M., Haspel, G., & Dobrowolski, R. (2017). TOR‐mediated regulation of metabolism in aging. Aging Cell, 16(6), 1219-1233. https://doi.org/10.1111/acel.12689

Bansal, A., Zhu, L. J., Yen, K., & Tissenbaum, H. A. (2015). Uncoupling lifespan and healthspan in Caenorhabditis elegans longevity mutants. Proceedings of the National Academy of Sciences, 112(3). https://doi.org/10.1073/pnas.1412192112

Barcelos, I. P. D., & Haas, R. H. (2019). CoQ10 and Aging. Biology, 8(2), 28. https://doi.org/10.3390/biology8020028

Bárcena, C., Mayoral, P., & Quirós, P. M. (2018). Mitohormesis, an Antiaging Paradigm. En International Review of Cell and Molecular Biology (Vol. 340, pp. 35-77). Elsevier. https://doi.org/10.1016/bs.ircmb.2018.05.002

Bentinger, M., Brismar, K., & Dallner, G. (2007). The antioxidant role of coenzyme Q. Mitochondrion, 7, S41-S50. https://doi.org/10.1016/j.mito.2007.02.006

Brenner, S. (1974). The genetics of *Caenorhabditis elegans*. Genetics, 77(1):71-94. doi: 10.1093/genetics/77.1.71.

Chaudhari, S. N., & Kipreos, E. T. (2017). Increased mitochondrial fusion allows the survival of older animals in diverse C. elegans longevity pathways. Nature Communications, 8(1), 182. https://doi.org/10.1038/s41467-017-00274-4

Choi, H. S., Bhat, A., Howington, M. B., Schaller, M. L., Cox, R., Huang, S., Beydoun, S., Miller, H. A., Tuckowski, A. M., Mecano, J., Dean, E. S., Jensen, L., Beard, D. A., Evans, C. R., & Leiser, S. F. (2021). FMO rewires metabolism to promote longevity through tryptophan and one carbon metabolism [Preprint]. Molecular Biology. https://doi.org/10.1101/2021.06.18.449022

Cohen, A. A., Ferrucci, L., Fülöp, T., Gravel, D., Hao, N., Kriete, A., Levine, M. E., Lipsitz, L. A., Olde Rikkert, M. G. M., Rutenberg, A., Stroustrup, N., & Varadhan, R. (2022). A complex systems approach to aging biology. Nature Aging, 2(7), 580-591. https://doi.org/10.1038/s43587-022-00252-6

Corona Velazquez, A. F., & Jackson, W. T. (2018). So Many Roads: The Multifaceted Regulation of Autophagy Induction. Molecular and Cellular Biology, 38(21), e00303-18. https://doi.org/10.1128/MCB.00303-18

Durieux, J., Wolff, S., & Dillin, A. (2011). The Cell-Non-Autonomous Nature of Electron Transport Chain-Mediated Longevity. Cell, 144(1), 79-91. https://doi.org/10.1016/j.cell.2010.12.016

Espinosa-Soto, C., Padilla-Longoria, P., & Alvarez-Buylla, E. R. (2004). A Gene Regulatory Network Model for Cell-Fate Determination during Arabidopsis thaliana Flower Development That

Is Robust and Recovers Experimental Gene Expression Profiles[W]. The Plant Cell, 16(11), 2923-2939. https://doi.org/10.1105/tpc.104.021725

Eureqa (1.24.0). (2015). [Software]. Nutonian Inc. http://52.45.171.32/products/eureqa-desktop/

Fumiã, H. F., & Martins, M. L. (2013). Boolean Network Model for Cancer Pathways: Predicting Carcinogenesis and Targeted Therapy Outcomes. PLoS ONE, 8(7), e69008. https://doi.org/10.1371/journal.pone.0069008

Gems, D., & De Magalhães, J. P. (2021). The hoverfly and the wasp: A critique of the hallmarks of aging as a paradigm. Ageing Research Reviews, 70, 101407. https://doi.org/10.1016/j.arr.2021.101407

Greer, E. L., & Brunet, A. (2009). Different dietary restriction regimens extend lifespan by both independent and overlapping genetic pathways in C. elegans. Aging Cell, 8(2), 113-127. https://doi.org/10.1111/j.1474-9726.2009.00459.x

Hart AC. Behavior. 2006 Jul 3. In: WormBook: The Online Review of C. elegans Biology [Internet]. Pasadena (CA): WormBook; 2005-2018. Available from: https://www.ncbi.nlm.nih.gov/books/NBK19734/

Haynes, C. M., Petrova, K., Benedetti, C., Yang, Y., & Ron, D. (2007). ClpP Mediates Activation of a Mitochondrial Unfolded Protein Response in C. elegans. Developmental Cell, 13(4), 467–480. https://doi.org/10.1016/j.devcel.2007.07.016

Hernando-Rodríguez, B., & Artal-Sanz, M. (2018). Mitochondrial Quality Control Mechanisms and the PHB (Prohibitin) Complex. Cells, 7(12), 238. https://doi.org/10.3390/cells7120238

Herndon, L. A., Schmeissner, P. J., Dudaronek, J. M., Brown, P. A., Listner, K. M., Sakano, Y., Paupard, M. C., Hall, D. H., & Driscoll, M. (2002). Stochastic and genetic factors influence tissue-specific decline in ageing C. elegans. Nature, 419(6909), 808-814. https://doi.org/10.1038/nature01135

Hwang, A. B., Ryu, E.-A., Artan, M., Chang, H.-W., Kabir, M. H., Nam, H.-J., Lee, D., Yang, J.-S., Kim, S., Mair, W. B., Lee, C., Lee, S. S., & Lee, S.-J. (2014). Feedback regulation via AMPK and HIF-1 mediates ROS-dependent longevity in Caenorhabditis elegans. Proceedings of the National Academy of Sciences, 111(42). https://doi.org/10.1073/pnas.1411199111

Institute for Systems Biology. (2019). Cytoscape. Retrieved from https://www.cytoscape.org

Kaeberlein, M. (2018). How healthy is the healthspan concept? GeroScience, 40(4), 361-364. https://doi.org/10.1007/s11357-018-0036-9

Kauffman, S. A. (1969). Metabolic stability and epigenesis in randomly constructed genetic nets. Journal of Theoretical Biology, 22(3), 437–467. https://doi.org/10.1016/0022-5193(69)90015-0

Khan, M. H., Ligon, M., Hussey, L. R., Hufnal, B., Farber, R., Munkácsy, E., Rodriguez, A., Dillow, A., Kahlig, E., & Rea, S. L. (2013). TAF-4 is required for the life extension of isp-1, clk-1 and tpk-1 Mit mutants. Aging, 5(10), 741-758. https://doi.org/10.18632/aging.100604

Lakowski, B., & Hekimi, S. (1996). Determination of Life-Span in Caenorhabditis elegans by Four Clock Genes. Science, 272(5264), 1010-1013. https://doi.org/10.1126/science.272.5264.1010

Lapierre, L. R., De Magalhaes Filho, C. D., McQuary, P. R., Chu, C.-C., Visvikis, O., Chang, J. T., Gelino, S., Ong, B., Davis, A. E., Irazoqui, J. E., Dillin, A., & Hansen, M. (2013). The TFEB orthologue HLH-30 regulates autophagy and modulates longevity in *Caenorhabditis elegans*. Nature Communications, 4(1), 2267. https://doi.org/10.1038/ncomms3267

Li, Y., Ding, W., Li, C.-Y., & Liu, Y. (2020). HLH-11 modulates lipid metabolism in response to nutrient availability. Nature Communications, 11(1), 5959. https://doi.org/10.1038/s41467-020-19754-1

Littlejohn, N. K., Seban, N., Liu, C.-C., & Srinivasan, S. (2020). A feedback loop governs the relationship between lipid metabolism and longevity. ELife, 9, e58815. https://doi.org/10.7554/eLife.58815

Liu, J.-L., Yee, C., Wang, Y., & Hekimi, S. (2017). A single biochemical activity underlies the pleiotropy of the aging-related protein CLK-1. Scientific Reports, 7(1), 859. https://doi.org/10.1038/s41598-017-00754-z

Long, N. P., & Kim, H. M. (2021). Distinct metabolic alterations in different *Caenorhabditis elegans* mitochondrial mutants. Journal of Chromatography B, 1179, 122863. https://doi.org/10.1016/j.jchromb.2021.122863

López-Otín, C., Blasco, M. A., Partridge, L., Serrano, M., & Kroemer, G. (2013). The Hallmarks of Aging. Cell, 153(6), 1194-1217. https://doi.org/10.1016/j.cell.2013.05.039

Mailler, E., Guardia, C. M., Bai, X., Jarnik, M., Williamson, C. D., Li, Y., Maio, N., Golden, A., & Bonifacino, J. S. (2021). The autophagy protein ATG9A enables lipid mobilization from lipid droplets. Nature Communications, 12(1), 6750. https://doi.org/10.1038/s41467-021-26999-x

Martinez-Sanchez M, Arias Del Angel J (2022). _BoolNetPerturb: Perturb Boolean Networks_. R package version 0.2.

Mayr, B., & Montminy, M. (2001). Transcriptional regulation by the phosphorylation-dependent factor CREB. Nature Reviews Molecular Cell Biology, 2(8), 599–609. https://doi.org/10.1038/35085068

Mendoza, L. (2006). A network model for the control of the differentiation process in Th cells. Biosystems, 84(2), 101-114. https://doi.org/10.1016/j.biosystems.2005.10.004

Munkácsy, E., & Rea, S. L. (2014). The paradox of mitochondrial dysfunction and extended longevity. Experimental Gerontology, 56, 221-233. https://doi.org/10.1016/j.exger.2014.03.016

Müssel, C., Hopfensitz, M., Kestler, H. (2010). BoolNet -- an R package for generation, reconstruction and analysis of Boolean networks. Bioinformatics 26(10):1378-1380.

Nakamura S, , Yoshimori T. (2018). Autophagy and Longevity. Mol. Cells 2018;41:65-72. https://doi.org/10.14348/molcells.2018.2333

Nguyen, T. B., Louie, S. M., Daniele, J. R., Tran, Q., Dillin, A., Zoncu, R., Nomura, D. K., & Olzmann, J. A. (2017). DGAT1-Dependent Lipid Droplet Biogenesis Protects Mitochondrial Function during Starvation-Induced Autophagy. Developmental Cell, 42(1), 9-21.e5. https://doi.org/10.1016/j.devcel.2017.06.003

Palikaras, K., Lionaki, E., & Tavernarakis, N. (2015). Coordination of mitophagy and mitochondrial biogenesis during ageing in C. elegans. Nature, 521(7553), 525-528. https://doi.org/10.1038/nature14300

Palikaras, K., Lionaki, E., & Tavernarakis, N. (2015). Coupling mitogenesis and mitophagy for longevity. Autophagy, 11(8), 1428–1430. https://doi.org/10.1080/15548627.2015.1061172

Park, H.-E. H., Jung, Y., & Lee, S.-J. V. (2017). Survival assays using Caenorhabditis elegans. Molecules and Cells, 40(2), 90–99. https://doi.org/10.14348/molcells.2017.0017

Rodríguez, A., Sosa, D., Torres, L., Molina, B., Frías, S., & Mendoza, L. (2012). A Boolean network model of the FA/BRCA pathway. Bioinformatics, 28(6), 858–866. https://doi.org/10.1093/bioinformatics/bts036

Rollins, J. A., Howard, A. C., Dobbins, S. K., Washburn, E. H., & Rogers, A. N. (2017). Assessing Health Span in Caenorhabditis elegans: Lessons From Short-Lived Mutants. The Journals of Gerontology: Series A, 72(4), 473-480. https://doi.org/10.1093/gerona/glw248

Schaar, C. E., Dues, D. J., Spielbauer, K. K., Machiela, E., Cooper, J. F., Senchuk, M., Hekimi, S., & Van Raamsdonk, J. M. (2015). Mitochondrial and Cytoplasmic ROS Have Opposing Effects on Lifespan. PLOS Genetics, 11(2), e1004972. https://doi.org/10.1371/journal.pgen.1004972

Schwab, J. D., Kühlwein, S. D., Ikonomi, N., Kühl, M., & Kestler, H. A. (2020). Concepts in Boolean network modeling: What do they all mean? Computational and Structural Biotechnology Journal, 18, 571-582. https://doi.org/10.1016/j.csbj.2020.03.001

Shaye, D. D., & Greenwald, I. (2011). OrthoList: A Compendium of *C. elegans* Genes with Human Orthologs. PLoS ONE, 6(5), e20085. https://doi.org/10.1371/journal.pone.0020085

Soetaert K., Petzoldt T., R. Setzer W. (2010). Solving Differential Equations in R: Package deSolve. Journa of Statistical Software, 33(9), 1--25. doi:10.18637/jss.v033.i09

Tissenbaum, H. A. (2012). Genetics, Life Span, Health Span, and the Aging Process in Caenorhabditis elegans. The Journals of Gerontology Series A: Biological Sciences and Medical Sciences, 67A(5), 503-510. https://doi.org/10.1093/gerona/gls088

Van Raamsdonk, J. M., Meng, Y., Camp, D., Yang, W., Jia, X., Bénard, C., & Hekimi, S. (2010). Decreased Energy Metabolism Extends Life Span in Caenorhabditis elegans Without Reducing Oxidative Damage. Genetics, 185(2), 559-571. https://doi.org/10.1534/genetics.110.115378

Wang, Y., & Hekimi, S. (2019). The Complexity of Making Ubiquinone. Trends in Endocrinology & Metabolism, 30(12), 929-943. https://doi.org/10.1016/j.tem.2019.08.009.

Wiedemann, N., & Pfanner, N. (2017). Mitochondrial Machineries for Protein Import and Assembly. Annual Review of Biochemistry, 86(1), 685–714. https://doi.org/10.1146/annurev-biochem-060815-014352

Wu, Z., Senchuk, M. M., Dues, D. J., Johnson, B. K., Cooper, J. F., Lew, L., Machiela, E., Schaar, C. E., DeJonge, H., Blackwell, T. K., & Van Raamsdonk, J. M. (2018). Mitochondrial unfolded protein response transcription factor ATFS-1 promotes longevity in a long-lived mitochondrial mutant through activation of stress response pathways. BMC Biology, 16(1), 147. https://doi.org/10.1186/s12915-018-0615-3

Yates, F. E. (1994). Order and complexity in dynamical systems: Homeodynamics as a generalized mechanics for biology. Mathematical and Computer Modelling, 19(6-8), 49-74. https://doi.org/10.1016/0895-7177(94)90189-9

Youle, R. J., & van der Bliek, A. M. (2012). Mitochondrial Fission, Fusion, and Stress. Science, 337(6098), 1062-1065. https://doi.org/10.1126/science.1219855

Zaarur, N., Desevin, K., Mackenzie, J., Lord, A., Grishok, A., & Kandror, K. V. (2019). ATGL-1 mediates the effect of dietary restriction and the insulin/IGF-1 signaling pathway on longevity in C. elegans. Molecular Metabolism, 27, 75–82. https://doi.org/10.1016/j.molmet.2019.07.001

Zhang, S., Li, F., Zhou, T., Wang, G., & Li, Z. (2020). *Caenorhabditis elegans* as a Useful Model for Studying Aging Mutations. Frontiers in Endocrinology, 11, 554994. https://doi.org/10.3389/fendo.2020.554994